Int. J. Heat Mass Transfer. Vol. 36, No. 5, pp. 1269–1285, 1993
Printed in Great Britain

0017-9310/93 $6.00 + 0.00

Burnout in highly subcooled water flow boiling in small diameter tubes

G. P. CELATA, M. CUMO and A. MARIANI
C.R.E. Casaccia, ENEA ENE-IMPE, Thermal Process Engineering Division,
Via Anguillarese, 301-00060 Rome, Italy

(*Received* 13 *January* 1992 *and in final form* 25 *May* 1992)

Abstract—The present work deals with the critical heat flux (CHF) in subcooled flow boiling in short tubes. The field of application is in the very high heat flux region (up to 60 MW m^{-2}) of interest to fusion technology (heat removal from divertors), which calls for a knowledge of the heat transfer under very high heat loading conditions. The experimental work was carried out with water at pressures ranging from 0.1 to 2.5 MPa and water velocities from 10 to 40 m s^{-1}, employing stainless steel 2.5 mm i.d. tubes. The heated length was 0.1 m ($L/D = 40$) and the wall thickness was 0.25 mm. The effects due to variation of thermal hydraulic parameters (velocity, subcooling, pressure) on the heat transfer are presented together with a comparison of the experimental data with existing correlations and theoretical models. The main result achieved in the experiment is the possibility of reaching such high values of the CHF using water in subcooled flow boiling inside smooth tubes. The parameters that seem to be determinant are the level of subcooling of the coolant and its velocity. Considering that other parameters, such as the tube diameter not investigated here, may have an influence on the CHF, it would also seem possible to come to the right compromise—with an optimized choice of parameters—between high values of the CHF and pressure loss involved (high with high velocity and small tube diameter) using this simple cooling technique.

INTRODUCTION

SUBCOOLED flow boiling has been widely investigated in the past [1–3]. As is well known, forced convection subcooled boiling involves a local-boiling liquid, whose bulk temperature is below the saturation, and that flows over a surface exposed to a high heat flux. It is one of the most efficient techniques of removing high heat fluxes. However, successful use of subcooled flow boiling with high heat flux requires the critical heat flux (CHF) to be avoided. A thorough review of CHF in subcooled flow boiling, with about 300 papers quoted, is given by Boyd [4, 5]. Studies performed so far have mainly referred to the thermal design of hot channels of light water reactors (LWRs). Consequently, the order of magnitude of the heat fluxes to be removed is around 1 MW m^{-2} (LWR heat flux of 0.06 MW m^{-2}). The range of interest of parameters such as pressure, liquid velocity and subcooling is around 15.0 MPa, 3–8 m s^{-1} and 25–50 K, respectively. Obviously, many existing data on CHF in subcooled flow boiling refer to the above reported ranges, with geometries varying from the single channel to the rod bundle, and L/D typical of LWRs ($L/D \sim 300$).

At present, fusion technology presents some of the most formidable engineering problems ever encountered by designers. One of them is related to the thermal hydraulics and particularly to the heat removal from components such as divertors, plasma limiters, neutral beam calorimeters, and ion dump and first-wall armour. The order of magnitude of the heat fluxes to be removed ranges from 2 to 80 MW m^{-2}. It is evident that we are more than an order of magnitude higher than in an LWR situation. Available data sets are therefore not suitable for the present problem, and existing theories often fail in describing the phenomenological behaviour.

Among the different possible techniques for the removal of such high heat fluxes, subcooled flow boiling turns out to be the most attractive for its simplicity as compared to hypervapotron [6–8], or high velocity helium gas convection and liquid metal heat transfer in the presence of a magnetic field [9] or subcooled flow boiling in swirl flow. Although significant data exist in subcooled flow boiling at high heat fluxes [4, 5], there is a scarcity of CHF data between 2 and 60 MW m^{-2}, for L/D from 25 to 500, under 'low' pressure, up to 5.0 MPa, high liquid velocity, up to 40 m s^{-1}, and high inlet subcooling, up to 200 K.

Existing CHF correlations and models for subcooled flow boiling, developed for LWR thermal hydraulics design purposes, are bound to present large errors in this range, and are generally unreliable because of their narrow ranges of parameters. As far as mechanistic models are concerned, complete understanding of the phenomena is far from being achieved, especially at low and intermediate pressures (up to 5.0 MPa). As reported by Celata [10], and also the few data published over the last four years, there is need for further experiments in the above reported range in order to: (a) obtain a relevant design data base that can be used in the development of design correlation for specific fusion components application; (b) enable the development of a mechanistic model of the CHF under these new conditions. Models may then be proposed to characterize not only the developing data

NOMENCLATURE

A	parameter defined in equation (6)
Bo	Boiling number, $q''/G\Delta h_v$
C	parameter defined in equation (3)
CHF	critical heat flux [MW m^{-2}]
C_p	specific heat [J kg^{-1} K^{-1}]
D	channel diameter [m]
F	parameter defined in equation (8)
G	mass flux [Mg m^{-2} s^{-1}]
g	gravitational acceleration [m s^{-2}]
$h, \Delta h$	enthalpy, enthalpy difference [J kg^{-1}]
h_l	heat transfer coefficient [W m^{-2} K^{-1}]
K	velocity coefficient [m s^{-1}]
k	thermal conductivity [W m^{-1} K^{-1}]
L	channel length [m]
l	5×10^{-6} m, typical height of surface micro-roughness
Δh_v	latent heat [J kg^{-1}]
L_a	entrance length [m]
L_B	vapour blanket length [m]
P	thermal power, in Table 1 [kW]
p	pressure, exit pressure in Table 1 [MPa]
q''	heat flux [MW m^{-2}]
R	parameter defined in equation (6)
Re	Reynolds number, GD/μ
t	wall thickness [m]
$T, \Delta T$	temperature, temperature difference [°C, K]
U_B	vapour blanket velocity [m s^{-1}]
U_δ	liquid sublayer velocity at δ [m s^{-1}]
u	liquid velocity [m s^{-1}]
x	quality.

Greek symbols

δ	liquid sublayer thickness [m]
μ	dynamic viscosity [kg m^{-1} s^{-1}]
ξ	parameter defined in equation (6)
$\rho, \Delta\rho$	density, density difference, $\rho_f - \rho_g$ [kg m^{-3}]
σ	stress, surface tension [kg cm^{-2}, N m^{-1}]
Ψ	parameter defined in equation (5).

Subscripts

adb	adiabatic conditions
CHF	pertains to critical heat flux conditions
conv	convective
ex	equilibrium conditions at the exit
exp	experimental
f	pertains to the liquid in saturated conditions
g	pertains to the vapour
i	inner
in	inlet
isp	inlet of test section
l	pertains to the liquid
o	outer
out	outlet
pb	pool boiling
sat	saturated
sub	subcooled, subcooling
tot	total
w	wall.

set, but also to be used for the prediction of the CHF beyond the data base limit, with reasonable reliability.

The present paper reports the results of an experimental investigation of CHF in highly subcooled water flow boiling, using a small diameter tube (2.5 mm) at water velocity up to 40 m s^{-1} and pressures up to 2.5 MPa.

EXPERIMENTAL APPARATUS

A schematic diagram of the water loop employed is drawn in Fig. 1. The loop was made of Type 304 stainless steel. The loop is filled with tap water passed through deionizing particulate beds (not shown in the figure). The alternative pump (a three-head piston pump), the maximum volumetric flow rate of which is 2000 l h^{-1}, is connected to a damper, to further reduce pressure oscillations whilst maintaining stable flow conditions (residual pulsation 2.5%). A turbine flow meter is installed to measure the water flow rate. The test section is always vertically oriented with water flowing upwards, even though other test section orientations and flow directions are possible. Test sections (one for each run) are made of Type 304 stainless steel (electric resistivity at 500 K is 93 $\mu\Omega$ cm), 2.5 ± 0.01 mm in i.d. and 0.25 mm in wall thickness, uniformly heated, over a length of 0.1 m, by the Joule effect using a 90 kW (50 V and 1800 A, d.c.) electric feeder. Of course, not all the electrical power is available for the test section, as it depends on the electrical resistance of this latter, which is, in turn, also a function of the temperature through the electrical resistivity. The test section is connected to copper feed clamps, by means of which it is possible to transfer the electric current to the tube. The power was computed by evaluating the product of the voltage drop across the test section and the current flowing through the walls of the test section. The current was computed from a measurement of the voltage drop (in mV) across a precision shunt resistor. Thermal expansion of the test section is mechanically allowed (~ 1.5 mm), thus preventing the rupture of the tube due to thermally induced compressive stresses. Before entering the test section, the water flows through an extension tube, of the same diameter as the test section, to assure that the liquid velocity profile is fully developed. The extension tube length is twice the entrance length, L_a,

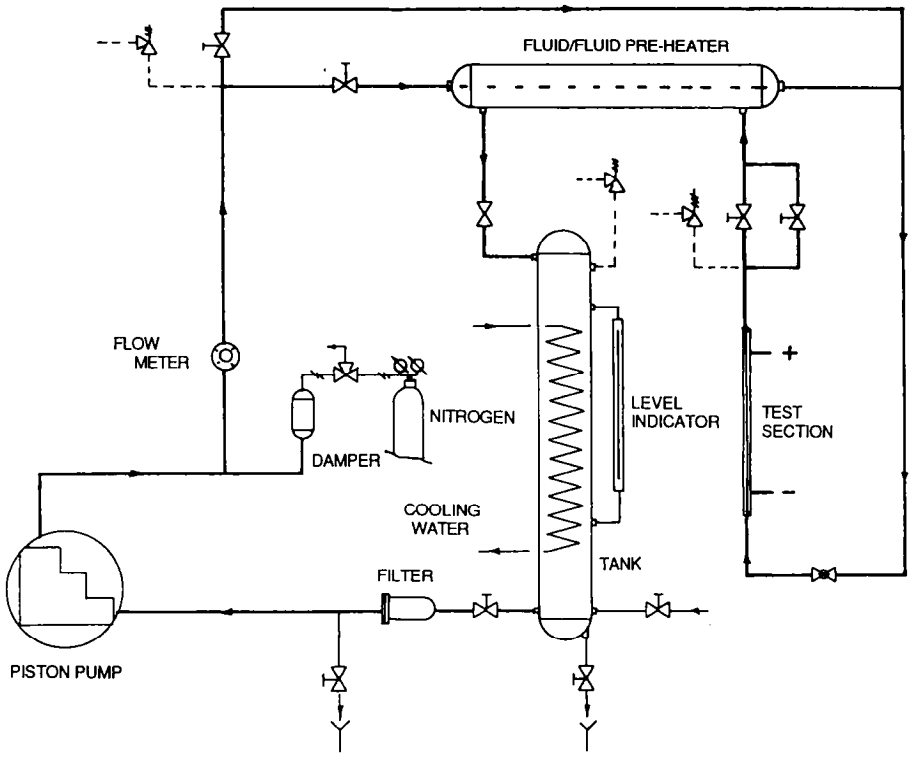

FIG. 1. Schematic of the experimental apparatus.

calculated under the most severe conditions (highest value of Reynolds number) using [11]:

$$\frac{L_a}{D} = 0.008\, Re^{0.685}. \quad (1)$$

Pressure taps are placed just upstream of the inlet of the unheated length of the test section, and just downstream of the exit of the heated length. The static pressure is measured by unsealed strain-gauge absolute pressure transducers. It is therefore possible to evaluate the pressure gradient in the test channel. The pressure at the exit of the test channel is regulated by an electrically controlled valve. The bulk fluid temperature is measured just upstream, $T_{f,in}$, and downstream, $T_{f,out}$, the latter after a suitable mixing of the liquid, of the test section using 0.5 mm K-type thermocouples. The knowledge of $T_{f,in}$ and $T_{f,out}$, together with the measurement of the water mass flow rate, allows the computation of the thermal power delivered to the fluid by the heat balance in the coolant. In fact, in all the tests performed (even at burnout conditions), the outlet bulk fluid temperature measurements always revealed the subcooling of the water at the exit of the test section. The employed test sections are not instrumented with wall thermocouples. Downstream of the test section, the fluid passes through the fluid-to-fluid pre-heater and then into the water cooled tank, where the fluid is cooled down to 25°C, even at the maximum thermal power delivered to the fluid, closing the loop through the filter, towards the piston pump. The maximum pressure of the loop is 7.0 MPa, while the maximum operating temperature of the pump is 70°C. The fluid-to-fluid pre-heater allows one to carry out experiments with a water inlet temperature above 70°C.

EXPERIMENTAL PROCEDURE

All the parameters are continuously monitored using digital and analogue displays, and each variation is recorded. The experimenal procedure consists of the following actions. First, the mass flow rate is set up using the manual control of the piston pump. Secondly, the exit pressure is established using the exit control valve. Once flow rate and exit pressure are steady, power is added to the test section. The control parameter used to approach the CHF is the electrical power delivered to the walls of the test section. The initial increment in the power is 0.5 kW. As the CHF is approached (70% of the expected value, obtained using the Gunther correlation, which is very simple and gives conservative predictions), the increment is reduced to 0.1 kW. After each increment, small adjustments are made in both the exit pressure and flow rate, so that the exit flow conditions correspond to the desired ones. The above reported procedure is repeated until burnout occurs, evidenced by test section destruction and detected by the sharp drop in

the electrical power. A computerized data acquisition system records the measured parameters at the occurrence of burnout.

EXPERIMENTAL RESULTS

In the present experiment, test conditions were selected by the combination of the following parameters: tube inner diameter, $D = 2.5 \pm 0.01$ mm; tube heated length, $L = 0.1$ m; wall thickness, $t = 0.25$ mm; water mass flux, G, 11–40 Mg m^{-2} s^{-1} (water velocity, u, 11–40 m s^{-1}); exit pressure, p, 0.6–2.5 MPa; inlet temperature, T_{in}, 30–70°C; inlet subcooling, $\Delta T_{sub,in}$, 96–210 K; outlet subcooling, $\Delta T_{sub,out}$, 50–136 K. Tests were carried out in order to verify the influence of a single parameter on CHF, i.e. variation of only that parameter with other conditions being fixed. Experimental results are summarized in Table 1, listing a total of 78 tests. The heat flux reported in Table 1 is obtained by the heat balance in the coolant, that is in subcooled conditions all along the test section, by measuring inlet and outlet liquid temperatures just upstream and downstream of the heated length of the test section. In this way heat loss from the test section is bypassed. W_e is the electrical power delivered to the test section as measured at the copper clamps and, therefore, does not account for heat loss. The CHF condition is defined as the heat flux corresponding to burnout, i.e. destruction of the test channel. Video films showed the existence, at burnout, of a narrow glowing area uniformly distributed around the perimeter, and located within 5 mm from the top copper feed clamp. Experimental results of CHF are reported in Fig. 2, where CHF is plotted versus mass flux, G, for different liquid inlet temperature values (top figure) and for the two extreme pressures (minimum and maximum, bottom figure); in Fig. 3, where CHF is plotted versus inlet subcooling, $\Delta T_{sub,in}$, for different outlet pressures (top figure) and water velocities (bottom figure); in Fig. 4, where CHF is plotted versus exit pressure, p, for different inlet subcooling and water velocity; and, finally, in Fig. 5, where CHF is plotted versus G in a global representation, together with experimental data of Inasaka and Nariai [12], carried out in similar test conditions, a fit of Boyd's results [13, 14], and Celata *et al.*'s previous data [15]. The values of the parameters reported on the figures are the nominal ones.

From Fig. 2 it can be noticed that the highest value of CHF is 60.6 MW m^{-2} (bottom graph), and, within the investigated range of G, the CHF is noted to be an increasing linear function of the mass flux. A factor of about three in the CHF is obtained on passing from 12 to 40 Mg m^{-2} s^{-1}. It is obvious that, apart from the problem of increasing the pressure drop, higher values of the CHF could be obtained by further increasing the mass flux. A significant effect on the CHF is exerted by the liquid inlet temperature, i.e. the inlet subcooling, of course in the sense that at lower inlet temperature (higher subcooling), a higher CHF is obtained. The ratio between the maximum value of the CHF ($T_{in} = 30$°C) and the minimum one ($T_{in} = 70$°C) ranges from 1.6 (at $G = 11$ Mg m^{-2} s^{-1}) to 1.1 (at $G = 40$ Mg m^{-2} s^{-1}), while the absolute increase looks almost constant. This influence is quite relevant considering the reduced variation of the water inlet temperature, i.e. only 40°C. It is therefore noted that, by looking at the bottom graph of Fig. 2, there is no difference between pressure and inlet subcooling effect on CHF. In fact, since the inlet temperature is constant for all the tests reported in the figure, different pressures also mean different liquid subcooling. The separate effects of the single parameters will be shown and analysed in subsequent figures.

In Fig. 3, CHF is plotted against the inlet subcooling for different outlet pressures and constant liquid velocity (30 m s^{-1}, top graph) and for different liquid velocities and a constant outlet pressure of 0.8 MPa (bottom graph). The almost linear dependence of CHF on inlet subcooling is evident and, above all, the significant influence of this parameter, already outlined in the discussion of the previous figure. The direct influence of the pressure is shown in Fig. 4, where the CHF is plotted versus the outlet pressure for different values of liquid velocity and subcooling, showing a slightly increasing dependence on the pressure. The influence of the pressure, although in the sense of increasing the CHF as the pressure increases (we refer to the outlet pressure), is weak, at least if considered with reference to liquid velocity and subcooling. Anyway, in the investigated range, the effect of the pressure on the CHF is not of great importance in obtaining very high heat fluxes to be removed. None the less, higher pressures, other conditions being equal, allows one to obtain higher liquid subcoolings, and, indirectly, contribute to the enhancement of CHF. It must be taken into account, as reported by Boyd [4] and Celata [10], that CHF behaviour versus pressure shows the presence of a maximum value occurring around 16.0 MPa, even though this latter value turns out to vary with the mass flux.

At this point, an initial physical conclusion may be drawn: the liquid velocity and subcooling are two of the main parameters on which it is possible to act for the enhancement of CHF in subcooled flow boiling in tubes.

Figure 5 shows an overall representation of present data, data published by Inasaka and Nariai [12], by Boyd [13, 14], and previous data of Celata *et al.* [15]. The experiments of Inasaka and Nariai [12] were carried out using a vertical stainless steel tube of 3.0 mm i.d. (0.5 mm wall thickness) and 100 mm long at pressures of 0.35, 0.6 and 1.0 MPa, mass fluxes from 5.5 to 30 Mg m^{-2} s^{-1} and inlet temperatures ranging from 25 to 75°C. They show and confirm, in the investigated range, the weak influence of the pressure on CHF, confirming, on the other hand, the importance of liquid mass flux and subcooling. Inasaka and

Nariai's data look very consistent with ours, and the maximum value of CHF obtained is 44.5 MW m^{-2} (T_{in} = 31°C, G = 29.9 Mg m^{-2} s^{-1}, p = 0.68 MPa). Boyd [13, 14] carried out experiments on horizontal tubes of a copper–zirconium alloy (amzirc) using deionized water. The inner diameter of the tube was 3 mm (wall thickness around 0.5 mm), with a heated length of about 0.29 m (L/D = 96.6). An entrance length (unheated) of 40D was assured to allow full development of the liquid velocity profile. The inlet temperature was set at 20°C for all the tests [13, 14]. The tests reported in ref. [13] were conducted at 0.77 MPa (T_{sat} = 169°C) with the mass flux, G, ranging from 4.6 to 40.6 Mg m^{-2} s^{-1}, while experiments presented in ref. [14] were performed at 1.66 MPa (T_{sat} = 203°C) with G ranging from 4.4 to 32 Mg m^{-2} s^{-1}. The dependence of CHF on G appears almost linear, at least for a wide range of mass flux, while

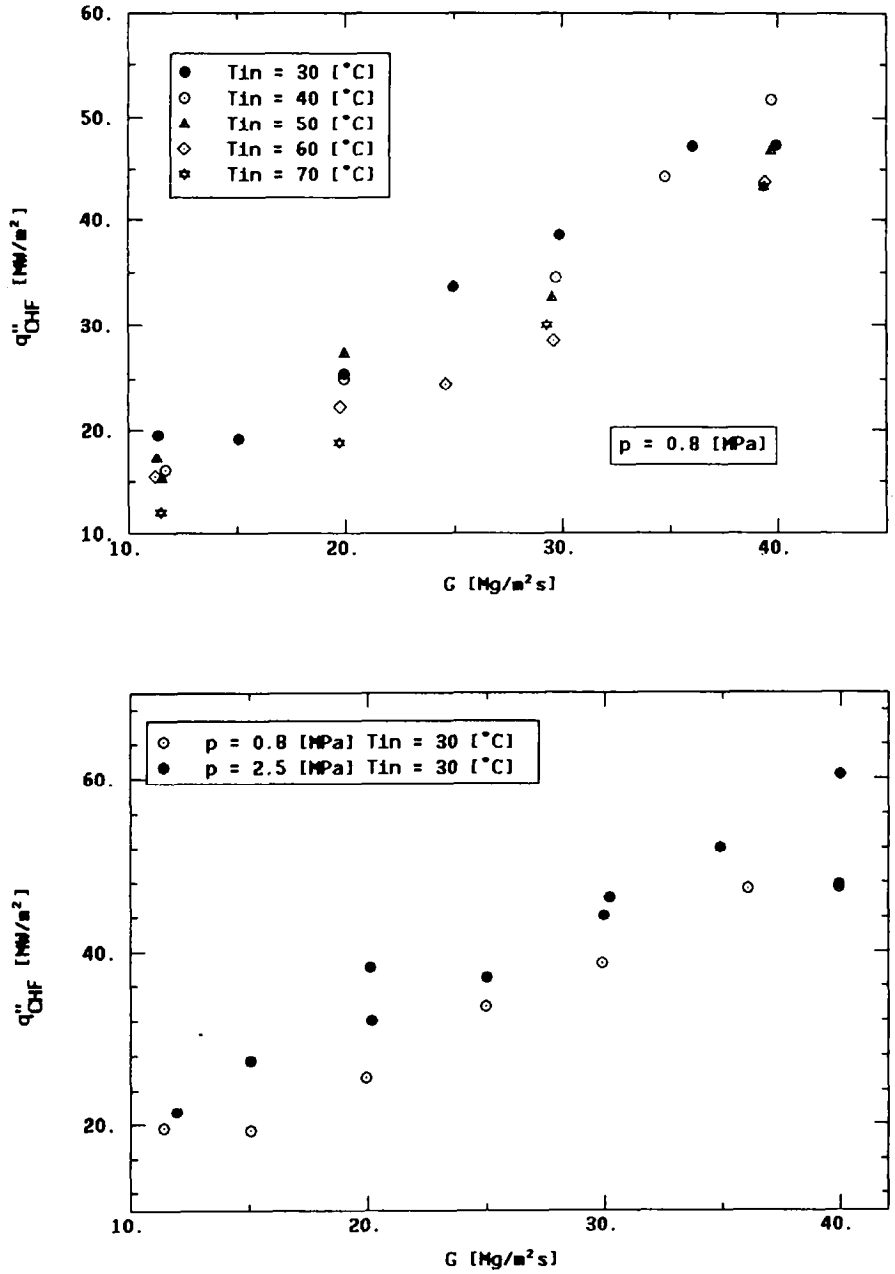

FIG. 2. CHF versus mass flux for different liquid inlet temperatures and constant pressure (top graph), and for different pressures and constant liquid inlet temperature (bottom graph).

Table 1. Experimental data

T_{in} [°C]	T_{out} [°C]	ΔT_{subin} [K]	ΔT_{subout} [K]	p_{in} [MPa]	p_{isp} [MPa]	p [MPa]	D [mm]	G [kg m^{-2} s^{-1}]	u_{out} [m s^{-1}]	w_e [kW]	q''_{CHF} [MW m^{-2}]	Name
30.28	98.28	144.69	72.97	0.9699	0.8918	0.8163	2.5	11390.0	11.868	15.904	19.57151	G3B2UA
30.04	101.37	193.70	121.09	2.5523	2.4906	2.4310	2.5	11949.8	12.470	20.116	21.49763	G3U2UA
40.76	94.95	128.85	70.95	0.8551	0.7848	0.7167	2.5	11690.2	12.152	16.453	16.10028	G4B2UA
48.25	100.66	124.57	69.03	0.9113	0.8477	0.7862	2.5	11516.8	12.022	12.668	15.33721	G5B2UA
49.79	110.65	119.59	55.43	0.8429	0.7803	0.7197	2.5	11303.5	11.892	16.209	17.38638	G5B2UA01
61.07	115.47	108.31	50.60	0.8429	0.7803	0.7197	2.5	11240.1	11.873	13.584	15.50084	G6B2UA
66.03	107.31	96.64	50.53	0.7403	0.6613	0.5849	2.5	11479.8	12.047	9.982	12.11245	G7B2UA
30.16	80.18	145.77	90.59	1.0212	0.9123	0.8069	2.5	15038.4	15.474	15.293	19.20938	I3B2UA
29.87	101.79	197.12	122.99	2.7574	2.6466	2.5394	2.5	15051.4	15.711	22.924	27.29309	I3U2UA
30.10	80.12	149.09	90.03	1.1799	0.9843	0.7951	2.5	19926.8	20.503	20.421	25.45108	M3B2UA
30.10	91.33	172.06	104.33	1.8417	1.6268	1.4189	2.5	20208.1	20.945	24.817	31.39202	M3H2UA
30.28	106.07	199.12	119.22	2.9772	2.7671	2.5639	2.5	20079.4	21.029	30.983	38.26931	M3U2UA
30.10	92.76	198.13	131.59	2.9040	2.7083	2.5191	2.5	20148.7	20.893	25.183	32.00307	M3U2UA01
40.06	89.14	140.83	83.01	1.2190	1.0233	0.8341	2.5	19926.6	20.627	21.093	24.93190	M4B2UA
40.47	104.10	148.99	77.25	1.4534	1.2404	1.0344	2.5	19856.8	20.780	27.015	31.92714	M4D2UA
40.59	103.15	161.95	93.32	1.8417	1.6393	1.4436	2.5	19996.5	20.907	26.404	31.63346	M4H2UA
40.64	94.00	165.90	105.39	2.0322	1.7797	1.5355	2.5	20066.3	20.836	22.680	27.22205	M4N2UA
40.53	96.38	167.50	105.41	2.0615	1.8340	1.6141	2.5	19998.9	20.801	21.947	28.35812	M4N2UA01
40.59	106.42	188.65	118.12	2.9968	2.7587	2.5285	2.5	20006.7	20.959	28.236	33.23780	M4U2UA
49.73	103.93	131.31	67.51	1.2410	1.0270	0.8201	2.5	19913.2	20.839	24.573	27.38696	M5B2UA
50.61	110.71	149.31	82.26	1.7733	1.5526	1.3392	2.5	19978.1	21.013	24.267	30.34980	M5F2UA
50.26	126.19	153.65	71.14	1.9101	1.6865	1.4702	2.5	19845.9	21.149	31.410	37.71111	M5H2UA
49.55	107.37	171.30	108.81	2.5670	2.3578	2.1556	2.5	20200.0	21.181	23.291	29.57747	M5S2UA
50.44	116.78	179.85	109.08	3.0407	2.8123	2.5914	2.5	19990.9	21.118	26.954	33.39925	M5U2UA
60.59	104.70	121.18	67.76	1.2556	1.0445	0.8404	2.5	19738.3	20.668	20.299	22.21087	M6B2UA
59.77	130.31	144.41	66.54	1.9443	1.6956	1.4551	2.5	19685.0	21.055	29.274	34.83139	M6H2UA
60.59	108.33	142.85	89.21	1.8710	1.6705	1.4767	2.5	19879.7	20.868	19.811	24.15632	M6L2UA
60.24	120.11	168.47	104.42	2.9430	2.7320	2.5278	2.5	19824.9	21.002	27.320	29.98732	M6U2UA
69.88	107.08	105.39	60.22	1.0602	0.8983	0.7418	2.5	19701.7	20.669	17.552	18.77868	M7B2UA
70.17	136.64	133.52	60.46	1.9027	1.6791	1.4629	2.5	19570.7	21.056	29.518	32.69592	M7H2UA
70.29	143.99	147.34	68.70	2.4278	2.2167	2.0126	2.5	19506.4	21.129	32.387	35.95841	M7Q2UA
70.47	146.50	149.36	68.40	2.5303	2.3125	2.1019	2.5	19910.9	21.620	31.471	37.80505	M7U2UA
30.16	83.15	156.17	89.32	1.4852	1.1575	0.8406	2.5	24954.4	25.726	26.099	33.70160	P3B2UA
30.28	88.54	201.09	136.82	3.1799	2.8686	2.5676	2.5	25041.2	25.889	29.151	37.07714	P3U2UA
60.36	99.23	125.28	73.37	1.4461	1.1396	0.8432	2.5	24635.6	25.688	21.459	24.50982	P6B2UA
30.28	80.89	160.70	92.19	1.7269	1.2826	0.8529	2.5	29913.0	30.793	31.716	38.63763	R3B2UA
30.46	92.88	172.72	97.87	2.0590	1.6610	1.2761	2.5	30053.5	31.185	35.928	47.54647	R3H2UA
30.16	88.25	199.18	132.16	3.2043	2.7639	2.3379	2.5	29933.7	30.944	37.027	44.18507	R3U2UA
30.93	91.27	194.44	124.86	2.9968	2.5679	2.1531	2.5	30199.3	31.288	38.858	46.24163	R3U2UA01
40.41	85.87	149.45	87.32	1.6610	1.2514	0.8553	2.5	29737.2	30.713	30.250	34.52941	R4B2UA
40.47	98.22	153.25	80.94	1.7513	1.3610	0.9835	2.5	29806.3	31.054	33.486	43.64510	R4D2UA
40.11	102.56	163.59	88.38	2.0908	1.6793	1.2813	2.5	30020.7	31.375	39.103	47.39631	R4H2UA
40.17	104.10	170.65	93.22	2.4253	1.9396	1.4698	2.5	29612.7	30.983	37.027	47.81860	R4H2UA01
40.29	107.79	170.15	89.35	2.4009	1.9248	1.4644	2.5	29816.9	31.287	43.559	50.72354	R4H2UA02
40.00	105.41	170.06	91.70	2.3716	1.9100	1.4635	2.5	29751.3	31.160	43.987	49.11642	R4H2UA03
40.23	114.87	172.47	83.07	2.5548	2.0131	1.4893	2.5	29819.6	31.469	44.719	55.83879	R4H2UA04
40.59	115.47	170.63	82.42	2.4375	1.9547	1.4877	2.5	29813.9	31.479	46.917	55.99679	R4H2UA05
40.41	114.99	169.96	82.81	2.3740	1.9220	1.4849	2.5	29815.2	31.468	47.711	55.78974	R4H2UA06
40.64	113.38	171.00	83.82	2.4937	1.9714	1.4662	2.5	29814.0	31.425	44.170	54.46769	R4H2UA07
40.06	110.59	166.61	82.36	2.2446	1.7839	1.3384	2.5	29817.6	31.360	44.109	52.90429	R4H2UA08
39.70	102.14	170.77	95.17	2.3985	1.9262	1.4695	2.5	29892.3	31.228	40.079	47.19458	R4H2UA09
40.17	119.46	170.34	77.72	2.4058	1.9278	1.4655	2.5	29818.3	31.590	46.306	59.13742	R4H2UA10
40.17	105.29	182.45	106.43	2.9186	2.4387	1.9745	2.5	29962.3	31.369	38.126	49.24973	R4N2UA
40.59	112.02	194.54	114.31	3.5413	3.0700	2.6143	2.5	29553.8	31.097	43.681	53.07256	R4U2UA
50.38	93.65	137.74	77.99	1.5975	1.2043	0.8240	2.5	29541.2	30.677	28.602	32.64619	R5B2UA
50.55	101.90	155.22	91.32	2.1714	1.7521	1.3467	2.5	29819.5	31.148	29.945	38.91664	R5F2UA
50.49	116.78	160.25	80.65	2.4156	1.9366	1.4733	2.5	29618.6	31.307	42.460	49.42593	R5H2UA
50.49	117.55	176.10	98.88	3.1042	2.6271	2.1658	2.5	29900.9	31.614	41.484	50.45828	R5S2UA
48.90	106.66	186.07	118.58	3.5780	3.0614	2.5618	2.5	29655.4	31.072	40.079	43.36914	R5U2UA
60.00	97.63	130.17	75.73	1.6756	1.2603	0.8585	2.5	29605.3	30.833	25.611	28.52667	R6B2UA
60.59	124.35	151.22	73.43	2.4888	1.9780	1.4840	2.5	29538.8	31.426	38.736	47.43462	R6H2UA
60.36	108.15	151.42	92.35	2.3960	1.9768	1.5713	2.5	29677.3	31.147	31.288	36.09780	R6L2UA
60.24	123.69	175.26	101.52	3.6390	3.0906	2.5603	2.5	29695.6	31.556	42.582	47.47463	R6U2UA
70.12	110.11	122.07	63.81	1.7782	1.3166	0.8701	2.5	29304.7	30.816	25.733	29.97141	R7B2UA
69.23	117.61	133.67	72.73	2.0517	1.6517	1.2649	2.5	29526.5	31.235	29.029	36.33979	R7H2UA
69.58	122.80	156.02	91.54	3.0969	2.5793	2.0788	2.5	29399.1	31.225	37.515	39.66689	R7Q2UA
69.88	138.97	165.86	86.70	3.6439	3.1042	2.5822	2.5	29333.6	31.609	45.513	50.84491	R7U2UA
30.34	81.66	165.54	92.12	2.0029	1.4256	0.8673	2.5	36044.0	37.122	38.675	47.18618	T3B2UA
30.87	89.55	206.36	136.08	3.8148	3.1874	2.5807	2.5	34895.7	36.102	43.620	52.00424	T3U2UA
40.41	90.32	152.47	79.39	1.9052	1.3366	0.7867	2.5	34748.6	36.001	35.806	44.17549	T4B2UA
59.65	119.76	177.38	105.18	3.8270	3.1765	2.5474	2.5	34267.2	36.291	41.239	52.00919	T6U2UA

Table 1 (*continued*)

T_{in} [°C]	T_{out} [°C]	ΔT_{subin} [K]	ΔT_{subout} [K]	p_{in} [MPa]	p_{isp} [MPa]	p [MPa]	D [mm]	G [kg m^{-2} s^{-1}]	u_{out} [m s^{-1}]	w_e [kW]	q''_{CHF} [MW m^{-2}]	Name
30.28	76.69	168.88	96.31	2.2275	1.5278	0.8512	2.5	39904.4	40.967	40.690	47.35876	V3B2UA
30.16	76.92	208.79	149.02	4.0004	3.2863	2.5956	2.5	39937.1	40.974	41.117	47.75323	V3U2UA
30.30	89.99	209.62	136.01	4.1142	3.3434	2.5979	2.5	39989.6	41.384	46.960	60.57851	V3U2UA01
40.53	91.75	163.92	83.59	2.5377	1.7050	0.8997	2.5	39697.4	41.167	41.422	51.73682	V4B2UA
50.26	96.62	152.63	78.66	2.4302	1.6515	0.8984	2.5	39666.8	41.280	40.446	46.86209	V5B2UA
60.36	103.93	141.88	72.62	2.3570	1.6293	0.9256	2.5	39399.0	41.228	35.440	43.78963	V6B2UA
69.82	112.97	127.91	58.42	2.1689	1.4827	0.8191	2.5	39323.3	41.448	31.288	43.29125	V7B2UA

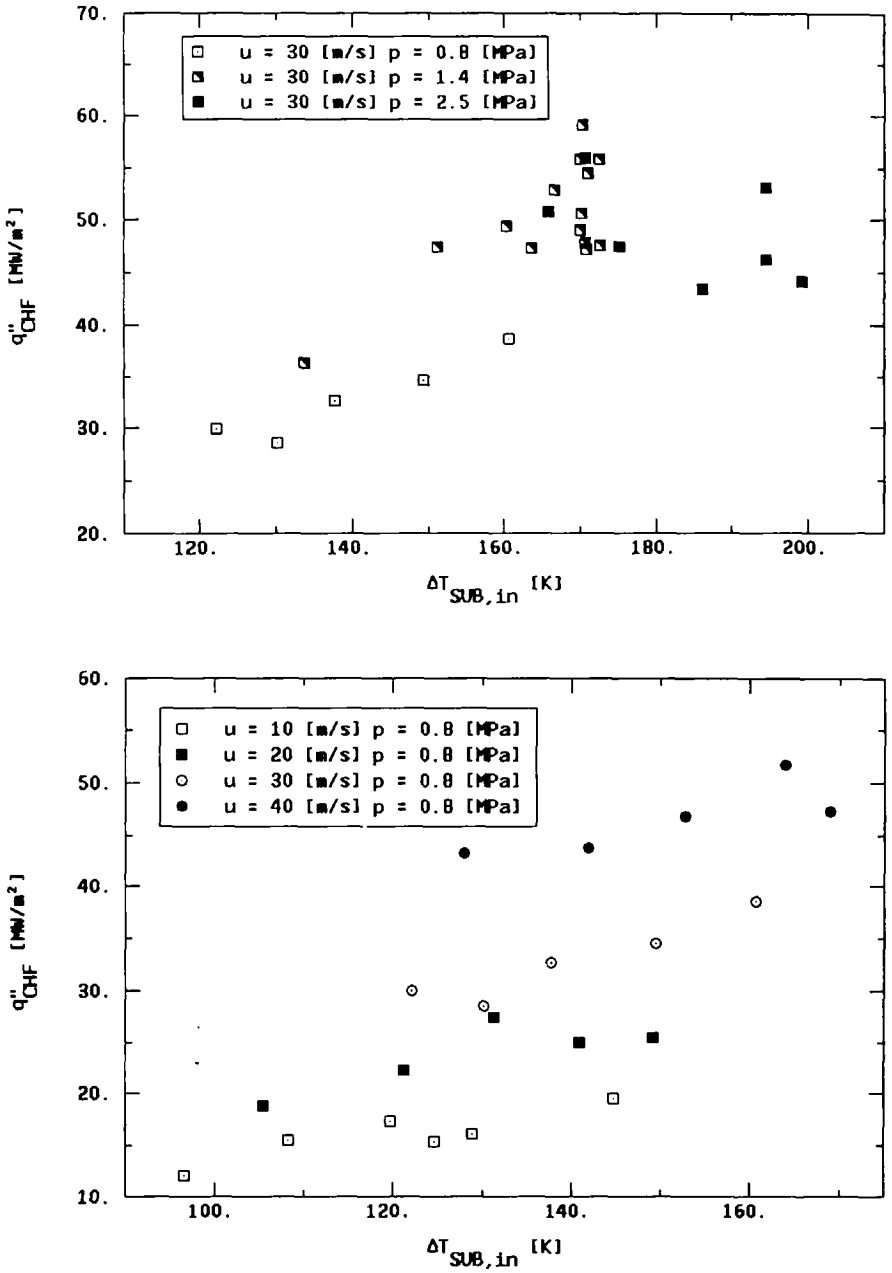

FIG. 3. CHF versus liquid inlet subcooling for different pressures and constant liquid velocity (top graph), and for different liquid velocities and constant pressure (bottom graph).

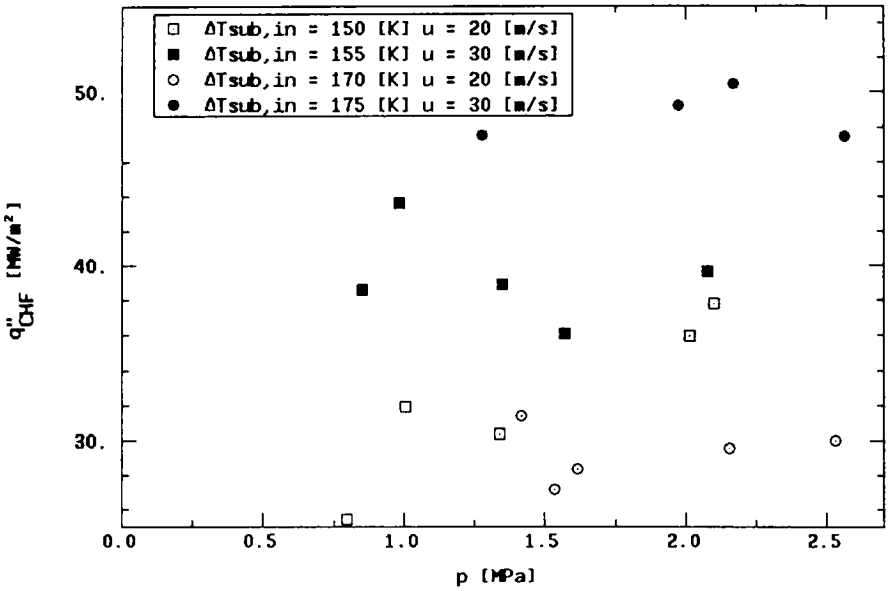

FIG. 4. CHF versus outlet pressure under similar inlet subcoolings and coolant velocities.

the exit pressure would seem to increase CHF. This conclusion could be spoiled by the different local subcoolings that the data have at different pressures, as Boyd kept the inlet temperature constant for all the tests. On the other hand, it was seen that the local subcooling is an important parameter, whilst the pressure, considering the range investigated by Boyd, should have a negligible effect. The maximum value of CHF obtained by Boyd is around 42 MW m^{-2} ($p = 0.77$ MPa, $G = 40.6$ Mg m^{-2} s^{-1}, $D = 3$ mm). The previous data of Celata *et al.* [15] (preliminary) were obtained using vertical stainless steel tubes of 2.5, 4.0 and 5.0 mm i.d., 0.25 mm wall thickness, and 100 mm length at pressures ranging from 0.1 to 2.2 MPa and mass fluxes of 2–33 Mg m^{-2} s^{-1}. Characteristics of the test rig did not allow control of the liquid inlet temperature (i.e. inlet subcooling), so experimental data did not provide the actual functional

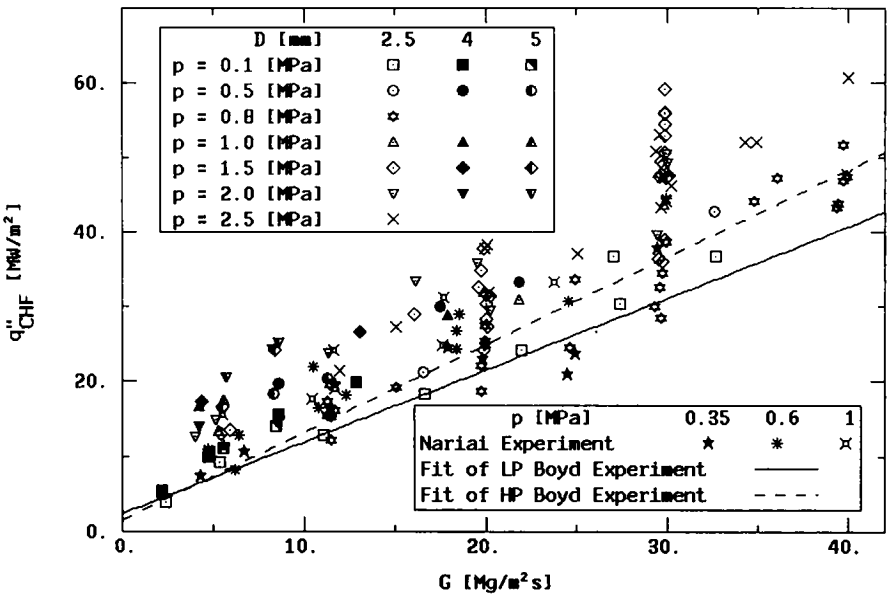

FIG. 5. Overall presentation of CHF data versus mass flux; present data, data from Inasaka and Nariai [12], Boyd [13, 14] and Celata *et al.* [15].

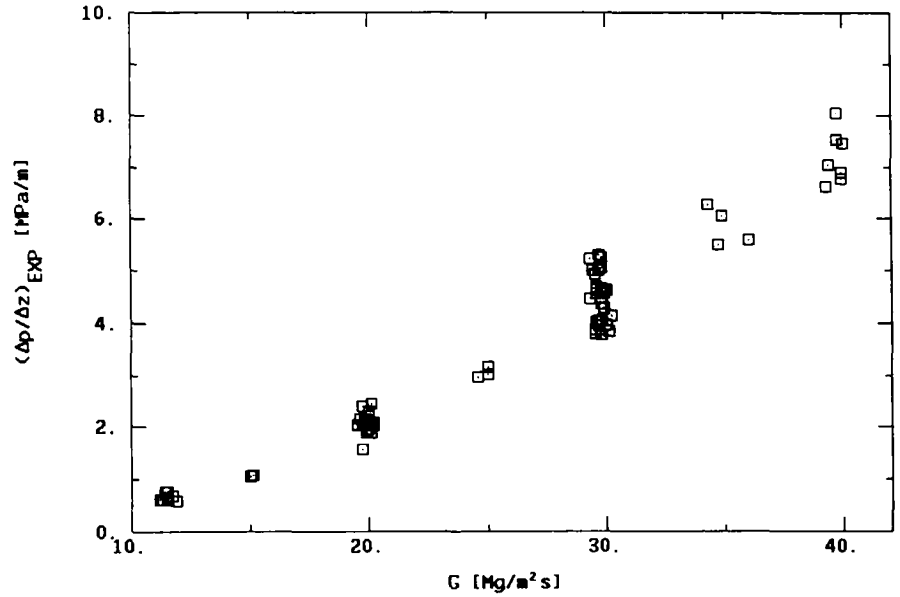

FIG. 6. Measured pressure gradient in the test channel versus mass flux.

dependence of CHF on the various parameters (p, G, D, ΔT_{sub}). The maximum CHF obtained was 42.7 MW m^{-2} ($G = 33.5$ Mg m^{-2} s^{-1}; $p = 0.49$ MPa; $\Delta T_{sub,in} = 164$ K; $D = 2.5$ mm).

Experimental results of pressure drop in the test section at burnout are reported in Fig. 6, where the pressure gradient is plotted versus the mass flux. The ratio between the experimental pressure drop in the test section, Δp_{exp}, and the calculated pressure drop in adiabatic conditions, Δp_{adb}, is plotted in Fig. 7 versus the critical heat flux. The friction factor used for the computation of Δp_{adb} has been determined experimentally in adiabatic conditions. Most of the experimental data of pressure drop are higher than the adiabatic values, especially when thermo-fluid dynamic conditions allow a consistent value of the subcooled void fraction. Other Δp_{exp} values are lower than the adiabatic ones because of the reduction of the water viscosity [16] (but also because of variations of other properties) due to the radial temperature

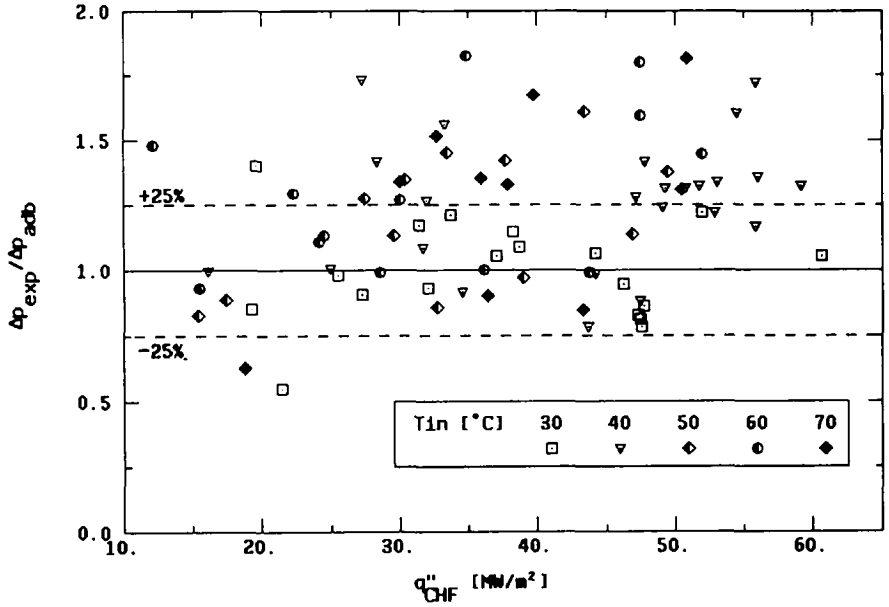

FIG. 7. Ratio of the experimental pressure drop at CHF and adiabatic pressure drop versus CHF.

profile that is highly peaked towards the wall. This latter effect may, in many cases, overcome that due to the presence of the bubbles close to the wall; the competition of these two effects gives rise to the results shown in Fig. 7.

A question could arise from the tests, i.e. whether the rupture of the tube is due to burnout or to a mechanical failure. In fact the relevant radial temperature gradient in the wall thickness (up to 1500°C mm^{-1}) gives rise to stresses that can drastically reduce the strength of the material. This could raise the doubt that the rupture of the heated channel may be of the mechanical type because of the internal pressure, even before the occurrence of burnout. Although the tube rupture zone is always accompanied by a narrow glowing area uniformly distributed around the perimeter that should mean occurrence of burnout, we carried out a mechanical verification of wall thickness stresses using the CASTEM 2000 code (developed by CEA and ENEA), which provides the finite element analysis of structures and components. The calculation was performed for the most critical cases in terms of pressure and of wall thickness thermal gradient, using the von Mises criterion. A first calculation done in the frame of the elastic field, plotted in Fig. 8, showed that the elastic limit of the AISI 304 stainless steel was by far exceeded. A calculation in the plastic field was therefore performed. Figure 9 reports typical results obtained, where the total stress, σ_{tot}, is plotted against the wall thickness (starting from the internal wall) for the case: $T_{wi} = 286$°C and $T_{wo} = 639$°C. The calculations show that most of the wall thickness is in the plastic regime ($\sigma_{tot} > 1250$ kg cm^{-1}); none the less, there is still a central region working in the elastic field. Considering that the calculation shown in Fig. 9 takes into account all the stresses, including those due to the pressure, and that the thermal stresses are of the secondary type (as they are generated by the local thermal dilatations), it may be concluded that

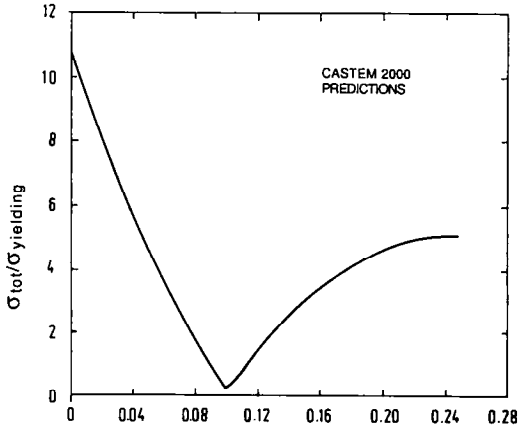

FIG. 8. Calculations of the total stress in the elastic field using the CASTEM 2000 code.

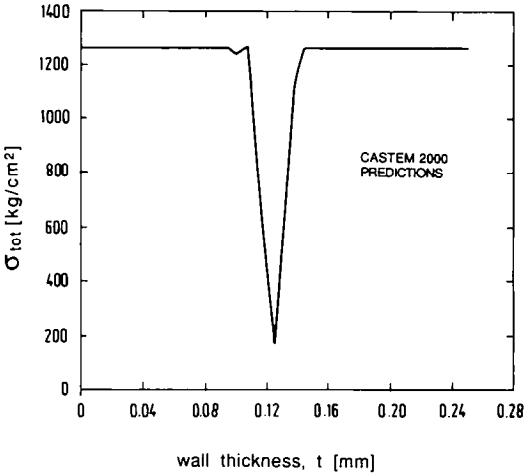

FIG. 9. Total stress versus wall thickness, calculated in the plastic field using the CASTEM code: $T_{wi} = 306$ C and $T_{wc} = 639$ C.

under these conditions the pipe should not undergo mechanical rupture. The outer wall temperature was obtained with an 'ad hoc' test carried out using a thermocamera AGEMA 870, while the inner wall temperature was evaluated knowing the thermal conductivity of stainless steel.

DATA REDUCTION

The results obtained so far, presented in the preceding section, are not sufficient to allow a deep and comprehensive analysis. Many other effects need to be investigated, such as higher pressure, orientation of the test channel, heated length and tube diameter, upflowing and downflowing, inlet subcooling, heat transfer along the test channel, and, above all, a visualization of the phenomenon with a high-speed camera, using an 'ad hoc' visualized test section. All of these items will be investigated in future steps of the research, with the aim of possibly developing a model of the phenomenon. For the time being, it is worth trying a comparison of the experimental data with predictions obtained using available correlations and models for the CHF in subcooled flow boiling. As there are no data in the range of interest, there is also a lack of suitable and reliable correlations for the prediction of subcooled CHF. The only possibility is to use available correlations that are recommended for ranges of validity completely different from the present data and evaluate the possibility of using them with a certain reliability outside the proposed ranges. Six correlations have been selected for comparison. All appear to give 'consistent' trends between predictions of the present and Celata *et al.*'s [15] experimental data.

Tong [17]

$$\frac{q''_{CHF}}{\Delta h_v} = C\frac{G^{0.4}\mu_f^{0.6}}{D^{0.6}} \tag{2}$$

$$C = 1.76 - 7.433x_{ex} + 12.222x_{ex}^2 \tag{3}$$

where Δh_v is the latent heat and μ_f is the dynamic viscosity of saturated liquid (SI units), while x_{ex} is the equilibrium quality at the exit. Tong's correlation may also be presented in the form

$$Bo = \frac{C}{Re^{0.6}} \tag{4}$$

where Bo and Re are the Boiling number and the Reynolds number, respectively. Because of its simple but comprehensive expression, which accounts for all parameters involved, we decided to modify the Tong correlation because of its systematic error in CHF prediction. A modification of this correlation was already accomplished by Inasaka and Nariai [12], but it still reveals a systematic overprediction of data as a function of pressure. That is probably due to the fact that in ref. [12] the Tong correlation was modified on the basis of very cold CHF data (with low values of CHF), in addition to a recent small data set by Inasaka and Nariai, which is in a very reduced range of pressure. We modified the parameter C, together with a slight modification of the Reynolds number power, to give a more accurate prediction in the range of pressures below 5.0 MPa, as the Tong correlation was recommended for pressures higher than 7.0 MPa. In addition to the present data, we also based the modification on data published in ref. [15] and on data with 6.0 and 8.0 mm i.d. tubes up to 5.0 MPa [18]. The new expression of the Tong correlation is

$$Bo = \frac{C}{Re^{0.5}} \tag{5}$$

with

$$C = (0.27 + 5.93 \times 10^{-2} p)\Psi$$

$$\Psi = 0.825 + 0.986 x_{ex} \quad \text{if } x_{ex} > -0.1$$

$$\Psi = 1 \quad \text{if } x_{ex} < -0.1.$$

The recommended region for the modified Tong correlation is the following: $D = 2$–20 mm; $L = 100$–200 mm; $p = 0.1$–20 MPa; $G = 1.3$–40 Mg m^{-2} s^{-1}: $q''_{CHF} = 2$–60 MW m^{-2}; $50 < \Delta T_{sub} < 150$ K, $-0.12 < x_{eq} < -0.46$, the latter being the equilibrium quality at the exit.

Avksentyuk [19]

$$q''_{CHF} = A \Delta h_v \rho_g^{0.5} (\sigma g \Delta \rho)^{0.25} \left[1 + 0.065 \left(\frac{\rho_f}{\rho_g} \right)^{0.8} \frac{\Delta h}{\Delta h_v} \right] + \frac{\rho_f u C_p (T_w - T_f) \xi / 8}{[1.07 + 12.7(\xi/8)^{0.5}(Pr^{0.66} - 1)]}$$

$$A = 7.5 \left[\left(\frac{g\sigma}{\Delta \rho} \right)^{0.25} \left(\frac{\rho_g}{\rho_f} \right)^{0.5} \right]^{0.5} \qquad \xi = (2 \log R + 1.74)^{-2}$$

$$R = 0.0625 Du \left(\frac{\rho_f}{l\sigma} \right)^{0.5} \qquad T_w = T_{sat} + \Delta T_w$$

$$\Delta T_w = 3.8 \times 10^2 \sigma^{7/16} T_{sat}^{0.5} (g \Delta \rho)^{3/16} \times (C_p K)^{-1/4} \rho_f^{-3/8} \quad \text{(calculated at } T_w\text{)} \tag{6}$$

where the physical properties in the last term (fraction) of equation (6), as well as in ξ and R, must be calculated at $(T_f + T_{sat})/2$; it is recommended in the ranges

$$2 < p < 20 \text{ MPa}; \quad 0 < \Delta T_{sub} < 75 \text{ K};$$

$$500 < G < 5000 \text{ kg m}^{-2} \text{ s}^{-1}.$$

Westinghouse [20]

$$q''_{CHF} = (0.23 \times 10^6 + 0.094G)(3 + 0.01 \Delta T_{sub}) \times [0.435 + 1.23 \exp(-0.0093 L/D)] \times \left\{ 1.7 - 1.4 \exp \left[0.532 \left(\frac{h_{sat} - h_{in}}{\Delta h_v} \right)^{3.4} \left(\frac{\rho_g}{\rho_f} \right)^{-1.3} \right] \right\} \tag{7}$$

recommended in the ranges

$$0.2 \times 10^6 < G < 8 \times 10^6 \text{ lb ft}^{-2} \text{ h}^{-1}$$

$$800 < p < 2750 \text{ psia}; \quad 21 < L/D < 365$$

$$h_{in} > 300 \text{ BTU lb}^{-1}; \quad 0 < \Delta T_{sub} < 228 \text{ F}$$

$$0.4 \times 10^6 < q''_{CHF} < 4 \times 10^6 \text{ BTU ft}^{-2} \text{ h}^{-1}$$

$(0.3 < G < 11 \text{ Mg m}^{-2} \text{ s}^{-1}; \quad 5.7 < p < 20.0 \text{ MPa};$

$1.25 < q''_{CHF} < 12.5 \text{ MW m}^{-2}; \quad 0 < \Delta T_{sub} < 126 \text{ K}).$

Levy [21]

$$q''_{CHF} = q''_{pb} + q''_{conv} + F$$

$$q''_{pb} = 0.131 \lambda \rho_g \left[\frac{\sigma^2 g (\rho_l - \rho_g)}{\rho_g^2} \right]^{1/4}$$

$$q''_{conv} = 0.696 (K \rho_l C_p)^{1/2} \left(\frac{\rho_l - \rho_g}{\sigma} \right)^{1/4} \times \left[\frac{\sigma^2 g (\rho_l - \rho_g)}{\rho_g^2} \right]^{1/8} \Delta T_{sub}$$

$$F = h_l (T_w - T_{sat}) + h_l \Delta T_{sub}$$

$$T_w - T_{sat} = \frac{60}{e^{p/900}} \left(\frac{q''}{10^6} \right)^{1/4}$$

$$h_l = 0.023 \frac{K}{D} Re^{0.8} Pr^{1/4} \tag{8}$$

recommended in the ranges $0.4 < G < 8 \times 10^6$ lb ft^{-2} h^{-1}; $60 < p < 2750$ psia; $0.075 < D < 0.5$ in, using British units ($0.6 < G < 11$ Mg m^{-2} s^{-1}; $0.4 < p < 20.0$ MPa; $2 < D < 12$ mm).

Gunther [22]

$$q''_{CHF} = 71987 u^{0.5} \Delta T_{sub} \quad [\text{W m}^{-2}], \tag{9}$$

where u (m s^{-1}) is the mean fluid velocity and ΔT_{sub} (K) is the liquid subcooling at the tube exit, rec-

ommended in the range $1.5 < u < 12.2$ m s^{-1}; $0.1 < p < 1.1$ MPa.

Knoebel et al. [23]

$$q''_{CHF} = 4.85 \times 10^5 (1 + 1.71 \times 10^{-4} G)(1 + 0.124 \Delta T_{sub}) \quad (10)$$

where ΔT_{sub} (K) is the liquid subcooling at the tube exit.

A comparison between the present experimental data and predictions obtained using the above six correlations is shown in Figs. 10 and 11, where the ratio between the experimental and the calculated CHF is plotted versus exit pressure. Additional data from the earlier studies of Celata *et al.* [15] are included. Of course, being modified on the present data set, the modified Tong correlation provides a reasonable prediction of the experimental data, with a maximum error of $\pm 25\%$ and good statistics. Among other correlations it is worth noting that two very old ones, the Westinghouse [20] and Levy [21] correlations, are able to predict CHF in highly subcooled conditions at high velocity with a more or less similar accuracy to the modified Tong correlation. The latter probably has the advantage of relatively major simplicity. The Gunther correlation [22] gives rise to a systematic overprediction of the present CHF data, the comparison tending to get worse as the pressure increases. The Knoebel correlation [23] provides a systematic underestimation of the experimental data, tending to an acceptable agreement for the higher pressures investigated. The Avksentyuk correlation [19] provides the worst prediction.

Known models have the advantage, with respect to correlations, of characterizing not only the existing and developing data base, but also for use in predicting CHF beyond the established data base. In this sense, visual information, not available in detail so far, would be of great help for a full understanding of the basic mechanisms of CHF in subcooled flow boiling at high liquid velocity and inlet subcooling, enabling the development of a mechanistic model of CHF more adherent to reality. At the moment, three different models are available in the literature for the prediction of the CHF in subcooled flow boiling: the Weisman–Ileslamlou [24], the Lee–Mudawar [25] and the Katto [26, 27] models.

The Weisman–Ileslamlou model (extension of the Weisman–Pei model [28]) is based on the existence of a bubbly layer adjacent to the heater surface. At the CHF, the bubbles agglomerate into a vapour blanket that prevents the liquid core from cooling the heater wall. It assumes that the turbulent interchange at the outer edge of the bubbly layer is the limiting mechanism. The void fraction in the bubbly layer was determined by a balance between the outward vapour flow away from the wall and the inward liquid flow at the bubbly layer–core interface. They postulated that CHF occurs when the void fraction in the bubbly layer just exceeds the critical value of 0.82. The void fraction was calculated under the assumption of homogeneous two-phase flow in the bubbly layer. With reference to the previous model description, the new one accounts for highly subcooling condition effects (energy balance at the bubbly layer–core interface), making the computation of the CHF an entirely local calculation (the authors claim that under subcooled and low quality conditions CHF is a local phenomenon). The authors tested and assessed their model within the following parameter ranges: $-0.12 > x_{ex} > -0.46$; $p = 6.8$–19 MPa; $D = 1.9$–37.5 mm; $L = 76$–1950 mm; $G = 1.3$–10.5 Mg m^{-2} s^{-1}.

The Lee–Mudawar model (liquid sublayer dryout model) is a mechanistic CHF model based on the observation that, during fully developed boiling, a vapour blanket forms in the vicinity of the heated wall by the coalescence of small bubbles, leaving a thin liquid sublayer in contact with the heated wall beneath the blanket. The onset of sublayer dryout was assumed to be triggered by a Helmholtz instability at the sublayer–vapour blanket interface, and CHF was postulated to occur when the rate of heat supplied at the wall exceeded the enthalpy of fresh liquid entering the sublayer from the bubbly layer and core regions (or, in other words, when the rate of sublayer mass loss by evaporation exceeded that of the liquid entering the sublayer from the core region). Although the model is mechanistic in nature, describing a specific process associated with CHF, its development requires the use of available correlations to describe the dynamics of bubbles in the wall region. The model was assessed by the authors (choice of correlations) in the following ranges of parameters: $p = 5$–17.6 MPa; $G = 1$–5.2 Mg m^{-2} s^{-1}; $D = 4$–16 mm; $\Delta T_{sub} = 0$–59 K.

The Katto model [26] is based on the same mechanism as the Lee–Mudawar model, i.e. it is a liquid sublayer dryout mechanism. A thin vapour layer or slug (called a 'vapour blanket') is formed due to accumulation and condensation of the vapour furnished from the wall, overlying a very thin liquid sublayer adjacent to the wall. CHF is assumed to occur when the liquid sublayer is extinguished by evaporation during the passage time of the vapour blanket sliding on it. Parameters to be determined in the description of the mechanistic model by Katto are: initial thickness of the sublayer, δ, vapour blanket length, L_B, and velocity, U_B. The evaluation of δ is obtained using a non-dimensional correlation derived in a previous study of CHF in pool boiling [29]. The vapour blanket length L_B is set equal to the critical wavelength of Helmholtz instability of the liquid–vapour interface. The vapour blanket velocity U_B is evaluated by relating it to the local velocity U_δ of the two-phase flow (which is assumed to be homogeneous flow) at a distance δ from the tube wall. U_δ is evaluated by the Karman velocity distribution and U_B is equal to KU_δ, where K is called the velocity coefficient and is the only quantity to be determined empirically in

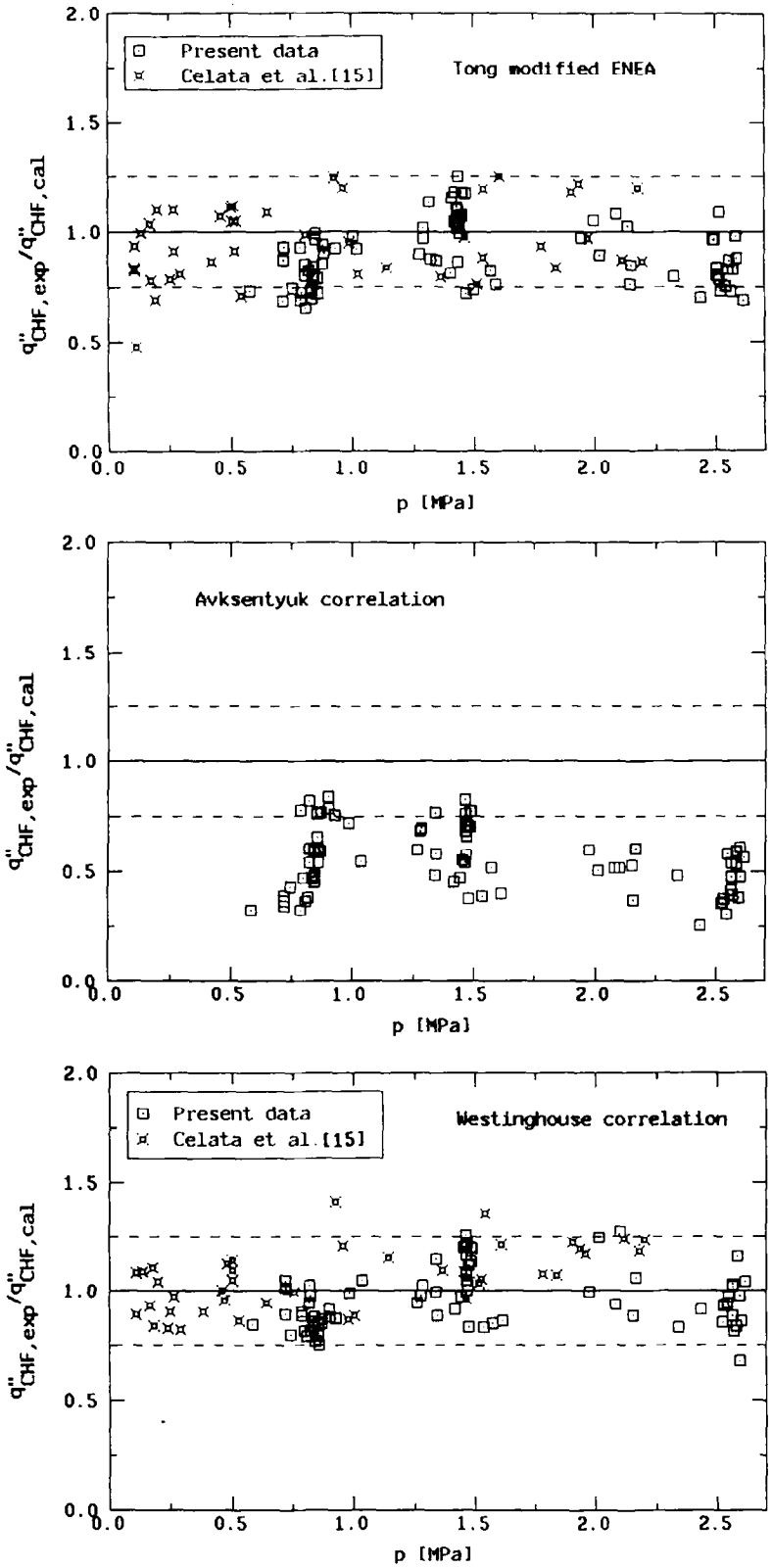

FIG. 10. Comparison between CHF data and predictions from Tong modified [17, 18], Avksentyuk [19] and Westinghouse [20] correlations.

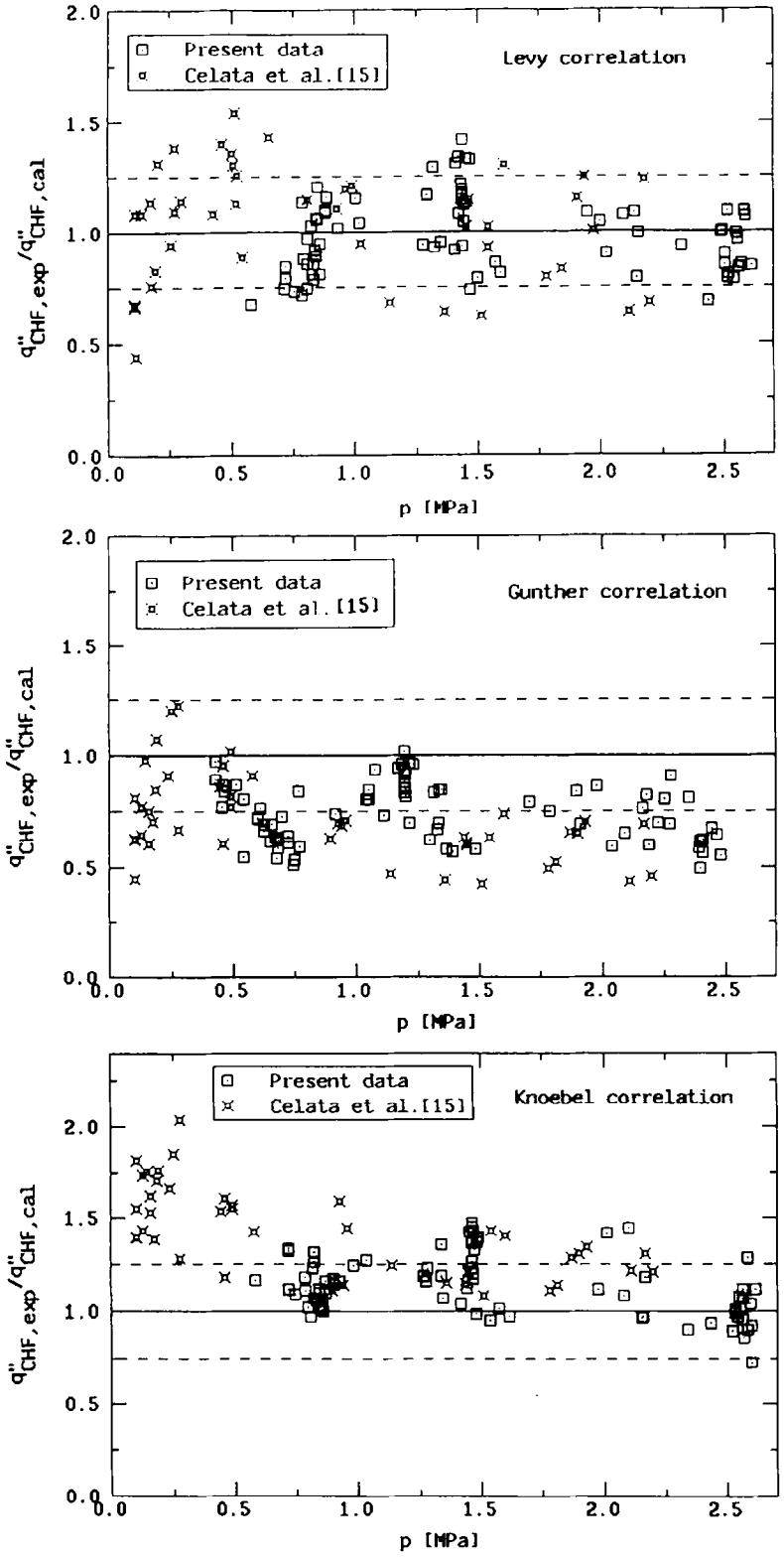

FIG. 11. Comparison between CHF data and predictions from Levy [21], Gunther [22] and Knoebel [23] correlations.

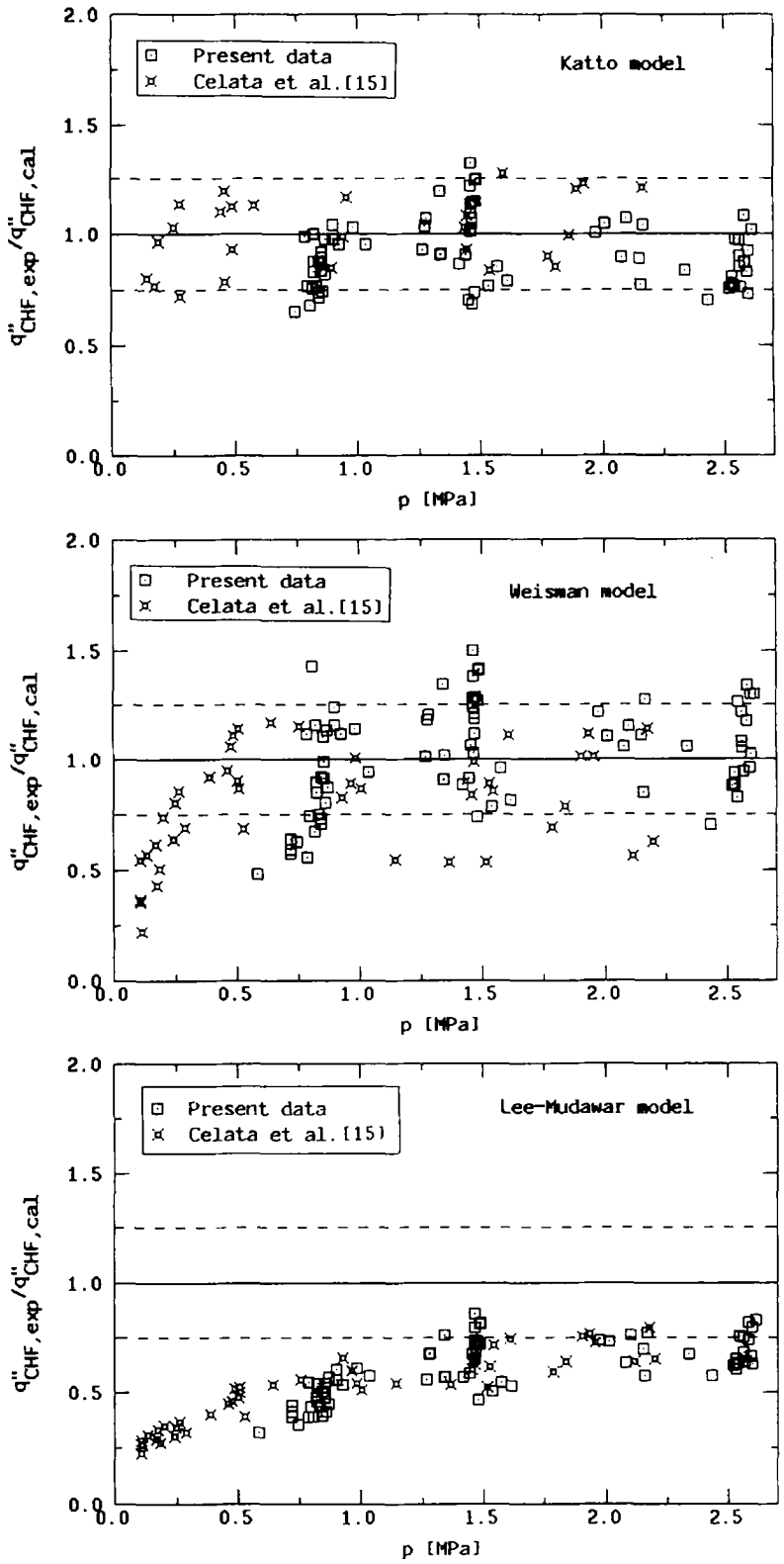

FIG. 12. Comparison between CHF data and predictions from Katto extended [30], Weisman–Ileslamlou [24] and Lee–Mudawar [25] models.

the Katto model. The velocity coefficient K was first derived on a limited data set obtaining a non-dimensional correlation as a function of Reynolds number, liquid and vapour density, and void fraction [26], then improved using other data sets [27] and finally extended to low pressures [30] using data reported in refs. [12, 14, 15]. The final version of the Katto model [30] was tested over the following range of parameters (water): $D = 1.14$–11.07 mm; $p = 0.1$–19.6 MPa; $G = 0.35$–40.6 Mg m^{-2} s^{-1}; $\Delta T_{sub,out} = 0$–117.5 K.

A comparison of predictions obtained using the above models with present and previous data [15] is shown in Fig. 12, where the ratio between the experimental and the calculated CHF is plotted against outlet pressure. The Weisman–Ileslamlou model gives predictions ranging within $\pm 50\%$, with a worst prediction at very low pressures (below 1.5 MPa). The Lee–Mudawar model exhibits a stronger systematic influence of the pressure (up to 2.0 MPa) coupled with a marked overprediction of the experimental conditions, even if a good collapse of data is shown. It must be considered that these two latter models are assessed, and therefore recommended, by the authors in their proposed version in a range of pressure above 7.0 MPa, and then outside the pressure range of present data. Good predictions are instead provided by the Katto model, which was assessed on a relatively low pressure data set (including data reported in ref. [15]), besides high pressure data.

Although mechanistic in nature, the three models presented above show the necessity of empirical parameters introduced in the mathematical description of the dynamics of the bubbles. Also the Katto model, which provides consistent predictions of the present data, introduces the velocity coefficient K, which must be derived from experiments. It is therefore still necessary to accomplish a full understanding of the phenomenon to propose a realistic and pure mechanistic model description.

CONCLUSIONS

(1) An experiment of critical heat flux was conducted at intermediate–low pressure (up to 2.5 MPa) and high mass fluxes (up to 40 Mg m^{-2} s^{-1}), with inlet subcoolings ranging from 96 to 210 K, using a stainless steel 2.5 mm i.d. tube, cooled with water in vertical upflow. High values of the CHF were achieved, ranging from 12.1 to 60.6 MW m^{-2}. Within the above range of parameters, the CHF exhibited the usual increasing function of coolant inlet subcooling and mass flux.

(2) These high values of heat flux are to be removed in nuclear fusion components, such as the divertor in the NET Programme. Subcooled flow boiling therefore appears suitable for removing high heat fluxes without employing techniques such as hypervapotron or twisted tape tubes, both requiring high pumping powers for the enormous pressure drop involved.

(3) Among the available subcooled CHF correlations and models there is the possibility of having a few of them upgraded to give acceptable predictions of the present data, even though more experiments are necessary (higher pressure and liquid velocity, orientation of the test channel, heated length and tube diameter, upflow and downflow, inlet subcooling, heat transfer along the test channel and above all visualization of the phenomenon). The aim is the creation of an understandable design data base that could be used either to derive design correlations for specific fusion component applications, or to develop a real mechanistic model for better understanding of the CHF under these new conditions, to characterize not only the developing data set but also for use in the prediction of the CHF beyond the data base limits, with reasonable reliability.

REFERENCES

1. A. E. Bergles, J. G. Collier, J. M. Delhaye, G. F. Hewitt and F. Mayinger, *Two-phase Flow and Heat Transfer in the Power and Process Industries*, pp. 226–255. Hemisphere, New York (1981).
2. J. G. Collier, *Convective Boiling and Condensation*, pp. 144–177. McGraw-Hill, New York (1981).
3. Y. Y. Hsu and R. W. Graham, *Transport Processes in Boiling and Two-phase Systems*, pp. 217–232. American Nuclear Society (1986).
4. R. D. Boyd, Subcooled flow boiling critical heat flux (CHF) and its application to fusion energy components. Part I: a review of fundamentals of CHF and related data base, *Fusion Technol.* **7**, 7–30 (1985).
5. R. D. Boyd, Subcooled flow boiling critical heat flux (CHF) and its application to fusion energy components. Part II: a review of microconvective, experimental, and correlational aspects, *Fusion Technol.* **7**, 31–52 (1985).
6. C. Beurtheret, Transfert de flux superieur a 1 kW/cm^2 par double changement de phase entre une paroi non isotherme et une liquide en convection forcee, *Proc. 4th Int. Heat Transfer Conf.*, Paper B 4.2, Paris (1970).
7. C. Beurtheret, A breakthrough in anode cooling systems: the hypervapotron, *Conf. on Electronic Device Techniques*, New York (September 1970).
8. A. Cardella, G. Cattadori, G. P. Celata and G. P. Gaspari, Heat transfer and burnout at high heat fluxes in subcooled water, European Two-phase Flow Group Meeting, Paper A3, Rome (27–29 May 1991).
9. R. D. Boyd, C. P. C. Wong and Y. S. Cha, Thermal-hydraulic assessment of high heat flux removal techniques for fusion applications, *Nuclear Engng Design* **88**, 103–110 (1985).
10. G. P. Celata, A review of recent experiments and prediction aspects of burnout at very high heat flux, *Keynote Lecture at the Int. Conf. on Multiphase Flows '91*, Tsukuba (24–27 September 1991).
11. M. Cumo, G. E. Farello and G. C. Pinchera, Determinazioni sperimentali della lunghezza di assetto fluidodinamico in canali a sezione circolare, *20th National Conf. ATI*, Genova (1965) [in Italian].
12. F. Inasaka and H. Nariai, Critical heat flux of subcooled flow boiling with water, *Proc. NURETH-4*, Karlsruhe, Vol. 1, pp. 115–120 (10–13 October 1989).
13. R. D. Boyd, Subcooled water flow boiling experiments under uniform high heat flux conditions, *Fusion Technol.* **13**, 131–142 (1988).
14. R. D. Boyd, Subcooled water flow boiling at 1.66 MPa under uniform high heat flux conditions, *ASME Winter Annual Meeting, HTD* Vol. 119, pp. 9–15.

15. G. P. Celata, M. Cumo, G. E. Farello and A. Mariani, Preliminary remarks on high heat flux CHF in subcooled water flow boiling, *Int. J. Heat Technol.* **8,** 20–42 (1990).
16. F. Inasaka, H. Nariai and T. Shimura, Pressure drops in subcooled flow boiling in narrow tubes, *Heat Transfer—Jap. Res.* **18,** 70–82 (1989).
17. L. S. Tong, Boundary-layer analysis of the flow boiling crisis, *Int. J. Heat Mass Transfer* **11,** 1208–1211 (1968).
18. G. P. Celata, Fundamental studies of CHF in highly subcooled water flow boiling—ENEA experimental facility and results, Specialists' Workshop on Divertor Plates Thermal-hydraulics, San Francisco (13–14 November 1991).
19. B. P. Avksentyuk, Critical heat fluxes with forced flow of subcooled and saturated liquids, *Therm. Engng* **35**(12), 694–697 (1988).
20. L. S. Tong, H. B. Currin and A. G. Thorp, An evaluation of the departure from nucleate boiling in bundles of reactor fuel rods, *Nucl. Sci. Engng* **33,** 7–15 (1968).
21. S. Levy, Prediction of the critical heat flux in forced convection flow, General Electric Report GEAP-3961 (1962).
22. F. C. Gunther, Photographic study of surface-boiling heat transfer to water with forced convection, *Trans. ASME* **73**(2), 115–123 (1951).
23. D. H. Knoebel, S. D. Harris, B. Crain, Jr. and R. M. Biderman, *Forced-convection Subcooled Critical Heat Flux*, DP-1306. E. I. Dupont de Nemours (February 1973).
24. J. Weisman and S. Ileslamlou, A phenomenological model for prediction of critical heat flux under highly subcooled conditions, *Fusion Technol.* **13,** 654–659 (1988) [Corrigendum in *Fusion Technol.* **15,** 1463 (1989)].
25. C. H. Lee and I. Mudawar, A mechanistic critical heat flux model for subcooled flow boiling based on local bulk flow conditions, *Int. J. Multiphase Flow* **14,** 711–728 (1988).
26. Y. Katto, A physical approach to critical heat flux of subcooled flow boiling in round tubes, *Int. J. Heat Mass Transfer* **33,** 611–620 (1990).
27. Y. Katto, Prediction of critical heat flux of subcooled flow boiling in round tubes, *Int. J. Heat Mass Transfer* **33,** 1921–1928 (1990).
28. J. Weisman and B. S. Pei, Prediction of the critical heat flux in flow boiling at intermediate qualities, *Int. J. Heat Mass Transfer* **26,** 1463 (1983).
29. Y. Haramura and Y. Katto, A new hydrodynamic model of critical heat flux, applicable widely to both pool and forced convection boiling on submerged bodies in saturated liquids, *Int. J. Heat Mass Transfer* **26,** 389–399 (1983).
30. Y. Katto, A prediction model of subcooled water flow boiling CHF for pressure in the range 0.1–20 MPa, *Int. J. Heat Mass Transfer* **35,** 1115–1123 (1992).